A multiscale model for hemodynamic properties' prediction after fenestrated endovascular aneurysm repair. A pilot study

Stavros Malatos[1], Anastasios Raptis[2], Michalis A. Xenos[1,2], George Kouvelos[3], Athanasios Katsargyris[4], Athanasios Giannoukas[2,3], Eric L. Verhoeven[4], Miltiadis Matsagkas[2,3]

[1]Department of Mathematics, Section of Applied Mathematics and Engineering Research, University of Ioannina, Ioannina, Greece
[2]Laboratory for Vascular Simulations, Institute of Vascular Diseases, Larissa, Greece
[3]Department of Vascular Surgery, Faculty of Medicine, School of Health Sciences, University of Thessaly, Larissa, Greece
[4]Department of Vascular and Endovascular Surgery, Paracelsus Medical University, Nuremberg, Germany

Abstract:

Aim: Fenestrated endovascular abdominal aortic aneurysm repair (FEVAR) has been increasingly applied for the treatment of anatomically suitable short-necked, juxtarenal, and suprarenal abdominal aortic aneurysms (AAA). Blood flow in the visceral vessels is maintained after FEVAR, but deployment of both the device and bridging covered stents might give rise to hemodynamic conditions that could impair the long-term success of the treatment. The aim of the present study is the development of a multiscale model that can reproduce hemodynamic flow in endograft models after FEVAR.

Methods: We reconstructed pre- and post-operative computed tomography scans of two patients treated with a custom-made fenestrated endograft. Blood flow properties were obtained by computational fluid dynamics (CFD) simulations for the post-FEVAR cases. Specifically, pressure drop, velocity, wall shear stress and mean helicity were measured during the cardiac cycle.

Results: No hemodynamic extremities with respect to the specialized wall shear stress (WSS) and helicity, based indexes were observed. A coherent helical field characterized blood flow topology during the cardiac cycle, with two counter-rotating helical structures. Regions of lowest time averaged WSS (TAWSS) in combination with high oscillatory shear index (OSI) are the areas after the splanchnic vessels at the aortic wall. Flow in the superior mesenteric and renal arteries remains almost unaffected after FEVAR. Important indices such as TAWSS, OSI and helicity are retained to almost normal levels. Low WSS values followed by high OSI values suggest that specific regions are sensitive to flow separation and probably to thrombus formation.

Conclusion: This pilot study shows the possibility of predicting non-invasively the hemodynamic performance of FEVAR utilizing CFD. FEVAR does not seem to alter target vessel and aorta perfusion significantly allowing good perfusion of visceral arteries.

INTRODUCTION

Fenestrated endovascular aneurysm repair (FEVAR) was first reported in 1999 for the treatment of a juxtarenal aortic aneurysm[1]. The technique was initially developed to treat high-risk patients unfit for open surgery and anatomically unsuitable for standard EVAR. Gradually, FEVAR has been increasingly applied for the treatment of all anatomically suitable short-necked, juxtarenal, and suprarenal aortic aneurysms. High volume centers have reported excellent perioperative and midterm outcomes[2,3]. However, FEVAR has also been associated with complications, such as loss of a visceral branch patency, stent fracture, endoleak, and graft migration[2-4].

Complications after FEVAR, such as target vessel thrombosis, could be associated to potential alteration in hemodynamics. Computational Fluid Dynamics (CFD) facilitates the identification of the hemodynamic conditions that might promote the advent of complications, focusing in regions of expected disturbances with high-resolution hemodynamics. Despite the increased popularity of CFD simulations in endovascular community, there are few studies delineating the hemodynamics in fenestrated endografts[5-8]. Additionally, Ou et al. highlighted hemodynamic variations in renal arteries with different stent orientations, concluding that appropriate cephalic deployment of a custom-made fenestrated endograft is a feasible strategy to preserve hemodynamic stability and durability[9]. Kandail et al. quantified the hemodynamic impact of flared renal stents on the performance of fenestrated endografts[2,4].

Author for correspondence:

Michalis A. Xenos

Assoc. Prof., Section of Applied Mathematics and Engineering Research, Department of Mathematics, University of Ioannina, Ioannina, Greece, 45110
Tel: +30 26510 008262,
E-mails: xenosmichalis@gmail.com, mxenos@uoi.gr
ISSN 1106-7237/ 2019 Hellenic Society of Vascular and Endovascular Surgery Published by Rotonda Publications

The modeling of such hemodynamic flows requires specialized multiscale models due to the complexity of physiology. There have been proposed holistic models of the arterial system[10,11]. Detailed three-dimensional time-dependent models have been developed, describing a particular part of the cardiovascular system. In these models the waveforms obtained from 1D / 0D models, used as boundary conditions for the 3D simulations[12,13]. The aim of the present study is the development of a multiscale model that can reproduce hemodynamic flow in endograft models after FEVAR.

MATERIAL AND METHODS

In this study, a multiscale model, composed of 1D and 3D parts that can reproduce hemodynamic flow in endograft models after FEVAR is presented. Through computational simulations, the blood flow in an indicative FEVAR case is characterized, drawing attention to the arteries that are supplied with blood through the fenestrations in the splanchnic vessels. The model provides high-resolution hemodynamic analytics, such as, time-averaged wall shear stress (TAWSS), oscillatory shear index (OSI), and local normalized helicity (LNH).

We studied the computed tomography (CT) scans, preoperatively and 1 month after FEVAR of 2 patients with a para-renal AAA treated electively by FEVAR. The patients underwent implantation of a custom-made fenestrated device at the Department of Vascular Surgery, Paracelsus Medical University, Nuremberg, Germany. Both patients gave written consent for utilization of the imaging data. The first patient underwent a double FEVAR (two fenestrations for the renal arteries and one scallop for the superior mesenteric artery, SMA). The second patient underwent FEVAR with three fenestrations (two for the renals and one for the SMA) and one scallop for the celiac axis, as depicted in Figure 1**.** Both patients received balloon expandable bridging stent-grafts in all target vessels.

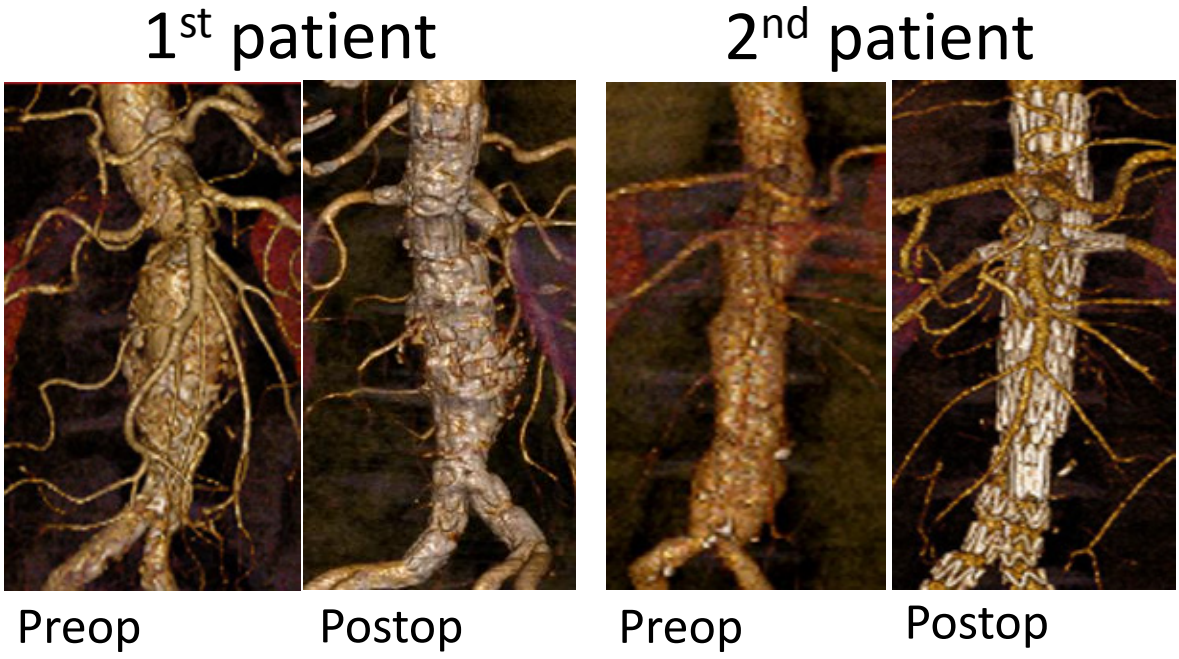

Figure 1. CT scans of the two patients pre- and post-operative cases.

3-dimensional patient-specific FEVAR model

Modelling approaches

The 3D model of the fenestrated stent-graft system, including the renal and superior mesenteric arteries and the celiac axis, was constructed using the CT scan of the treated patient. The reconstruction of the DICOM images into a three-dimensional model that preserves the geometry of the lumen postoperatively, was performed in the image processing and reconstruction software, Mimics (Materialise, Leuven, Belgium). The reconstructed geometry of the fenestrated endograft was subsequently meshed with tetrahedral elements in the software package ICEM CFD (Ansys Inc., Canonsburg, PA). After mesh independence test, a numerical grid of 2 million cells was considered sufficient to accurately predict the hemodynamic flow in detail.

Governing equations

The numerical simulations were performed in the software package Ansys Fluent (Ansys Inc., Canonsburg, US). Blood was considered as Newtonian fluid with density, ρ=1050 Kg/m^3 and kinematic viscosity, ν = 3.2×10^{-6} m^2/s. The unsteady and incompressible blood flow is governed by the coupled non-linear system of transport equation such as the continuity and Navier-Stokes equations:

$$\begin{cases} \nabla \cdot \boldsymbol{u} = 0, \\ \dfrac{\partial \boldsymbol{u}}{\partial t} + (\boldsymbol{u} \cdot \nabla)\boldsymbol{u} = -\dfrac{1}{\rho}\nabla p + \nu \nabla^2 \boldsymbol{u}, \end{cases} \qquad (1)$$

where **u** is the velocity vector, ν is the kinematic viscosity, ρ is the density and *p* is the blood pressure.

Boundary conditions for the 3D model

1-dimensional holistic model

To perform CFD simulations, boundary conditions are required at the inlet and outlets of the model. The 3D model of the fenestrated endograft has one inlet, at the suprarenal abdominal aorta, and several outlets, at the superior mesenteric artery, celiac axis, renal arteries and common iliac arteries. Given the lack of patient-specific information regarding flow or pressure at the inlet and the outlets, we developed a 1D model that can provide the required waveforms at the points of interest for subsequent use in the 3D hemodynamic simulations. Specifically, the 1D model is composed of a system of elastic cylindrical tubes that enables the mathematical description of blood flow in an extended subset of the arterial system, as displayed in Figure 2a. The tubes are inter-connected with each other, meaning that the outflow from the preceding tube defines the inflow to the succeeding one, along with appropriate conditions at bifurcations[10,14]. As initial conditions the pressure and the flow waveforms in the ascending aorta were introduced in the model. The 1D model can predict for each vessel the flow (q), pressure (p) and cross-sectional area (A). The model relies on literature data for the definition of the Young's modulus, E, on each tube, while the wall thickness, h, and base diameter, A_0 of each segment are patient-based. To include blood flow through the microvascular system (smaller arteries, arterioles and capillaries), a lumped-parameter model (3-element Windkessel) is attached at each end of the network of tubes[13]. Figure 2 shows a graphical representation of the multiscale model that relies on 0D, 1D parts to export boundary condition for the high-resolution 3D hemodynamic simulations after FEVAR.

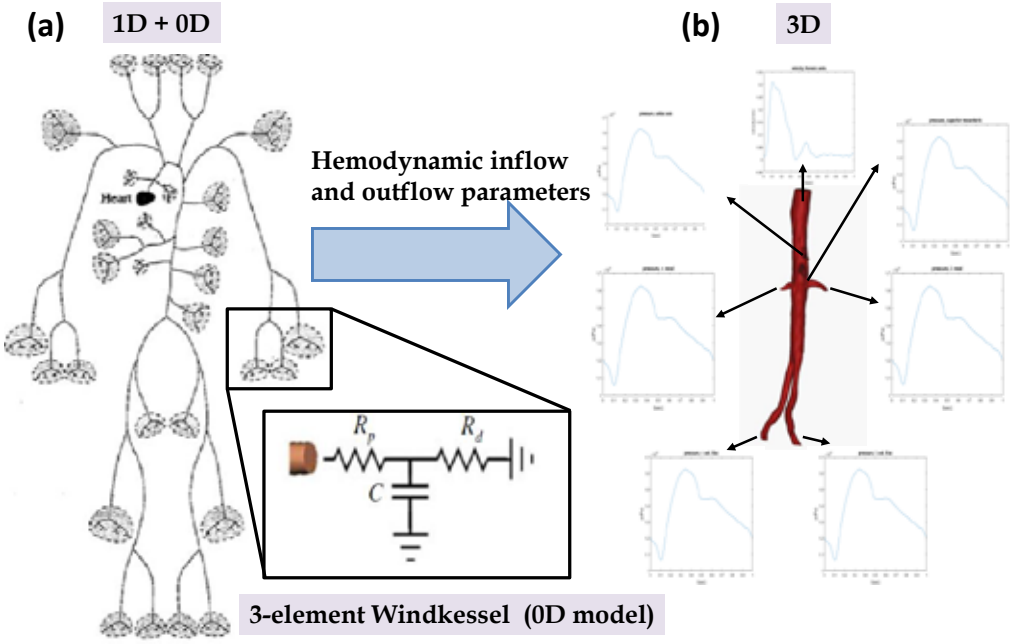

Figure 2. The multiscale arterial blood flow model.

Numerical solution

The governing partial differential equations[1] of blood flow are discretized with the Finite Volume method. The resulting system of algebraic equations is solved iteratively using the SIMPLE pressure-velocity coupling scheme and convergence was achieved when residual error of each equation was equal to 10^{-5}. The cardiac cycle was considered to last 1s, with a fixed time step of Δt = 0.0035s. The simulations were performed for four cardiac cycles in two Intel Xeon processors (E5645, 2.40GHz, 12MB Cache, 5.86GT/s Intel QPI) of a Dell™ Precision™ T7500 workstation. We exclusively utilized the results of the fourth cardiac cycle avoiding any dynamic disturbances of the numerical solution in the initial three cycles.

Hemodynamic parameters

WSS-related properties. Besides wall shear stress (WSS), additional WSS-derived properties were calculated. Specifically, the hemodynamic analysis includes the time averaged wall shear stress (TAWSS) over a cardiac cycle,

$$\mathrm{TAWSS}(\boldsymbol{s}) = \frac{1}{T}\int_0^T |WSS(\boldsymbol{s},t)|\,dt, \qquad (2)$$

and the oscillatory shear index (OSI),

$$\mathrm{OSI}(\boldsymbol{s}) = 0.5\left[1 - \frac{\frac{1}{T}\left|\int_0^T WSS(\boldsymbol{s},t)\,dt\right|}{\frac{1}{T}\int_0^T |WSS(\boldsymbol{s},t)|\,dt}\right], \qquad (3)$$

where *T* is the duration of cardiac cycle, ***s*** the generic location at the vessel wall and *t* is time[15,16].

Helicity-related parameters. Helicity, *H(**s**, t)*, is an index applied to quantify the interplay between rotational and trans-

lational motion of blood and is defined as the scalar product of the velocity field ***v(s, t)*** and the vorticity field, ***ω(s, t)*** at a location, ***s,*** in the flow field[17,18]. The local normalized helicity (LNH) is defined as,

$$\mathrm{LNH} = \frac{\boldsymbol{v}(\boldsymbol{s},t)\cdot\boldsymbol{\omega}(\boldsymbol{s},t)}{|\boldsymbol{v}(\boldsymbol{s},t)\cdot\boldsymbol{\omega}(\boldsymbol{s},t)|}. \qquad (4)$$

The quantity LNH, is a function of space and time and is an indicator of the intensity of helical structures and their direction of rotation[17]. Specifically, when the absolute value of LNH is one, then the flow is purely helical, and when it is zero, blood flow is characterized symmetric. The sign of LNH dictates the right or left-handed direction of the rotation of helical structures.

RESULTS

The proposed multiscale model of the arterial system is able to provide information on the flow, pressure and changes in the cross section of the entire arterial system, Table 1. It can be used to describe significant hemodynamic phenomena based on appropriate non-invasive patient-based measurements.

Arteries	Mean Flow, q *(ml/s)*	Mean Arterial Pressure, p *(mm Hg)*	Cross-sectional variation, A (%)
Ascending aorta	99.8	95.91	3.53
R. subclavian & brachial	7.49	86.88	4.90
R. com. carotid	7.49	78.21	6.21
Aortic arch (I)	84.91	95.01	3.68
Thoracic aorta	70.13	93.97	4.09
Celiac axis	0.54	93.85	4.11
Superior mesenteric	10.11	90.06	4.73
Abdominal aorta (II)	59.47	93.42	3.75
R. renal	10.72	87.71	5.06
R. com. & external iliac	19.66	90.50	2.44
R. Internal iliac	4.53	79.57	1.16
R. Femoral	15.13	86.54	2.10

Table 1. Quantification of mean flow, mean blood pressure and percentage change in cross-sectional area, as derived from the model in basic arteries during the cardiac cycle.

WSS-related parameters. The spatial WSS profile at peak systole is displayed in Figure 3. It is shown that low WSS magnitude applies on the main body of the stent-graft, WSS < 10 Pa, and higher WSS, in the range of 15-40 Pa, is observed along the surface of the limbs, Figure 3 (a). On the wall of renal arteries, celiac axis and superior mesenteric arteries, the magnitude of WSS is in the range of 30-35 Pa, Figure 3 (b)-(e).

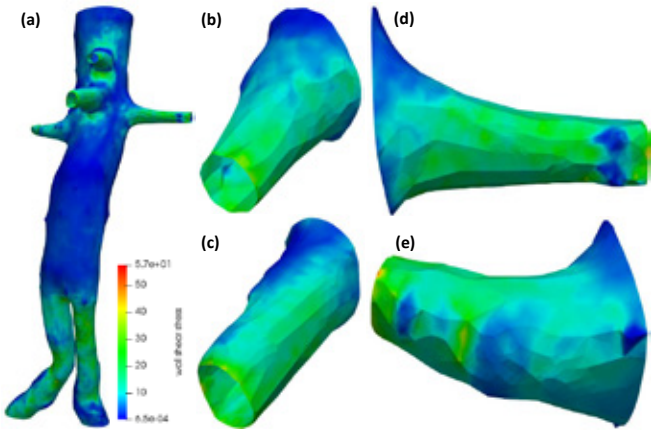

Figure 3. Wall shear stress at the maximum of the systolic phase. (a) WSS in extended graft (abdominal and iliacs), (b) WSS in the celiac axis, (c) WSS in the superior mesenteric artery, (d) WSS in the left renal artery, and (e) WSS in the right renal artery.

The distribution of TAWSS on the surface of the lumen showed that areas with higher values appear in the smaller arteries, iliacs, mesenteric, celiac axis and renal arteries, in the range of 4 - 8Pa, while smaller values of 2 - 4Pa, Figure 4 (a), are observed on the main body of the device. In the superior mesenteric, celiac axis and renal arteries, Figure 4 (b)-(e) the value of TAWSS ranges from 2 - 9 Pa**.**

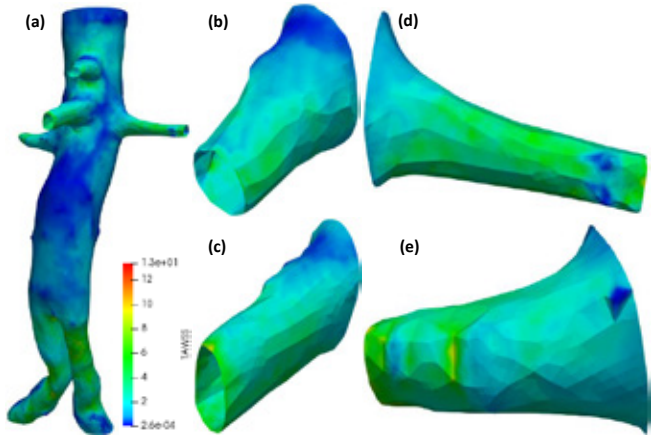

Figure 4. The profiles of time-averaged wall shear stress, (TAWSS) during cardiac cycle. (a) TAWSS throughout the graft (abdominal and iliacs), (b) TAWSS in the celiac axis, (c) TAWSS in the superior mesenteric artery, (d) TAWSS in the left renal artery and (e) TAWSS in the right renal artery

The OSI has been proposed as a parameter that can give an estimate of in-graft thrombus formation risk in correlation with WSS and TAWSS[19] and characterizes whether the WSS vector is aligned with the TAWSS vector throughout the cardiac cycle. Elevated OSI levels are often accompanied by low TAWSS, and together they serve as indicators for vascular injury or dysfunction[20], as depicted in Figure 5. An OSI value close to zero (OSI < 0.2) indicates that flow is unidirectional at that location throughout the pulsatile cycle whereas a high OSI value (OSI > 0.2) indicates that the flow oscillates forward

and backward for the same periods of time during the entire cardiac cycle[21]. At high OSI values blood flow induces the retrograde flow, causing a greater change in flow direction near the wall. In addition, this regions has a higher probability of developing lesions, as OSI values>0.2 trend to the development of endothelial dysfunction. Thus, OSI is a relatively sensitive hemodynamic indicator of regional vascular remodeling. In Figure 5, the areas in the renals mesenteric, celiac axis and iliac arteries exhibits low OSI. On the contrary regions such as the entrance of these arteries and a large portion of the aortic lumen reveal an intense OSI.

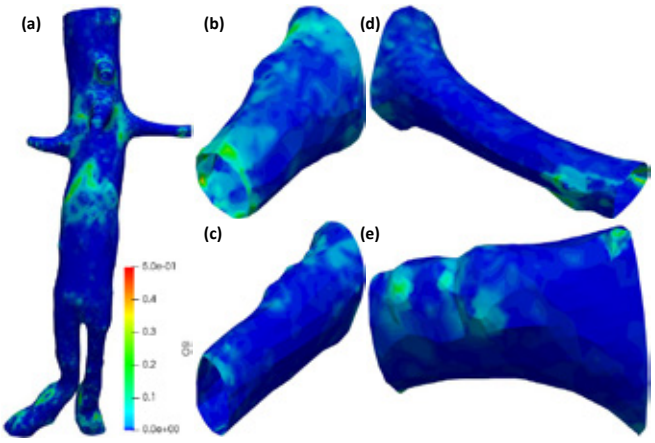

Figure 5. The profiles of oscillatory shear index (OSI) during cardiac cycle. (a) OSI throughout the graft (abdominal and iliacs), (b) OSI in the celiac axis, (c) OSI in the superior mesenteric artery, (d) OSI in the left renal artery and (e) OSI in the right renal artery.

Helicity-related parameters. In the main body of the fenestrated device there are two, almost uniformly distributed helical structures in different directions, Figure 6 (a). In the smaller arteries and at the entrance of the graft, these helical structures are separated into individual smaller structures, Figure 6 (b)-(e). The order of average helicity is |LNH|≤0.2.

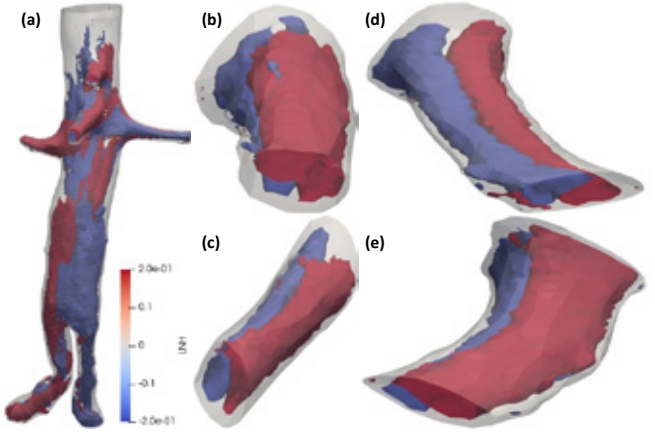

Figure 6. The local normalized helicity (LNH) during the cardiac cycle. (a) LNH throughout the graft (abdominal and iliacs), (b) LNH in the celiac axis, (c) LNH in the superior mesenteric artery, (d) LNH in the left renal artery, and (e)) LNH in the right renal artery.

The above hemodynamic indices are similar for the two patients, so we have decided to highlight the results obtained from one of the two patients. We observe that the second patient exhibits slightly lower WSS values in the abdominal part of the stent-graft, the remaining part exhibits similar behavior. The second patient also presents lower OSI values but similar LNH behavior with the first patient.

DISCUSSION

FEVAR has matured and became a valid alternative to open surgery, especially in high-risk surgical patients. In the short term, FEVAR success largely depends on the accurate preoperative planning, and the appropriate device design[22], while in the long-term, it seems important to maintain graft integrity to avoid complications such as target vessel thrombosis or endograft's migration. Data obtained by CFD simulations may theoretically aid to improve those devices and eventually lead to a better long-term outcome.

CFD simulations may aid to evaluate the durability of fenestrated stent-grafts and seem cost-effective and reliable when used in conjunction with physiologically correct boundary conditions[4]. In recent years, a number of multiscale approaches have been proposed to accurately describe blood flow dynamics of compliant arterial vessels[11,13,23]. Multiscale models are widely used as boundary conditions for advanced 3D patient-based models through simple Windkessel or lumped models for the rest of the circulation. Simplified 1D models, have been coupled with 3D model to determine the hemodynamic characteristics and represents a significant step forward for realistic representation of the cardiovascular system[24-28]. In this study, a multiscale model was developed composed of a 1D simplified model to describe blood circulation. The data from the simplified model are used as boundary conditions for advanced 3D patient-based FEVAR models. For the microvascular system, a lumped-parameter model is attached at each end of the circulation network. This pilot study shows the possibility of predicting non-invasively the hemodynamic performance of FEVARs utilizing CFD.

The notion of wall shear stress (WSS) is important in the clinical practice due to the fact that a pathological profile of shear stresses can impede atherogenesis, thrombosis, adhesion of leukocytes, smooth muscle proliferation and endothelial apoptosis[29]. Additionally, the parallel action of high and low shear stresses at the aortic wall in connection with irregularities of the lumen, could initiate the activation of the platelets that could eventually lead to thrombosis[30-33]. For the stented cases, the presence of low shear stresses might lead to in-stent restenosis and possibly to limb occlusion that in turn will force the patient to undergo additional intervention[29]. In previous studies has been shown that the postoperative structures reveal a reduction in the maximum WSS in the abdominal part of the graft compared to the normal cases[34,35]. Additionally, TAWSS has a significant difference between repaired and healthy cases during the cardiac cycle[36]. The combination of TAWSS and OSI could reveal regions more susceptible to thrombus formation due to flow separation. The results of the present study demonstrate that the regions

characterized by the lowest TAWSS in combination with high values of OSI are the areas after the splanchnic vessels at the abdominal aortic wall.

Helical flow has been reported to play a positive role facilitating blood flow transport, suppressing disturbed blood flow, preventing accumulation of atherogenic lipoproteins on the arterial surfaces, enhancing oxygen transport from the blood to the arterial wall, thus reducing the adhesion of blood cells on the surface[37]. The helical arrangement of the flow visualized at renals, superior mesenteric and celiac axis, has its energetic meaning in the compensative attempt of curling the forward blood flow, to fill the space due to flow separation at the wall. The results of the present study indicate that a coherent helical field characterizes blood flow topology during the entire cardiac cycle, with two counter-rotating helical structures[17]. Additionally, a high level of LNH is instrumental in suppressing low velocity/stagnation regions leading to a healthy flow profile in the FEVAR. In a nutshell, the study reveals no significant changes according to the hemodynamic indices. The clinical outcome of this pilot study is that FEVAR does not alter target vessel and aorta perfusion significantly allowing good perfusion of visceral arteries. Additional study including a large cohort of patients is required to infer unquestionable clinical implications.

Limitations

The elastic properties of the graft material were not taken into account in the 3D patient-based structure and the surface of the lumen was modeled as rigid. Blood could be modeled as non-Newtonian fluid, separating red blood cells from plasma, which were considered in the current study as a single continuum medium. The geometric and structural parameters employed in the 1D arterial model was based on bibliographic data. A future arterial model could be constructed with a geometry and elasticity database derived from patient-based measurements, and the model predictions would be compared with non-invasive measurements.

CONCLUSION

The findings of this study show that the flow in the superior mesenteric and renal arteries remains almost unaffected after FEVAR retaining all important indices to normal levels. However, low values of WSS followed by high values of OSI could suggest that these regions are more sensitive to flow separation and may become prone to thrombus formation.

Conflict of Interest

E.L.G.V. is consultant for Cook and Atrium.

REFERENCES

1 Browne T, Hartley D, Purchas S, Rosenberg M, Van Schie G, Lawrence-Brown M. A fenestrated covered suprarenal aortic stent. European journal of vascular and endovascular surgery. 1999;18(5):445-9

2 Kandail HS, Hamady M, Xu XY. hemodynamic Functions of Fenestrated stent graft under resting, hypertension, and exercise conditions. Frontiers in surgery. 2016;3:35

3 Verhoeven EL, Katsargyris A, Oikonomou K, Kouvelos G, Renner H, Ritter W. Fenestrated Endovascular Aortic Aneurysm Repair as a First Line Treatment Option to Treat Short Necked, Juxtarenal, and Suprarenal Aneurysms. European journal of vascular and endovascular surgery : the official journal of the European Society for Vascular Surgery. 2016

4 Kandail H, Hamady M, Xu XY. Effect of a Flared Renal Stent on the Performance of Fenestrated Stent-Grafts at Rest and Exercise Conditions. Journal of Endovascular Therapy. 2016;23(5):809-20

5 Suess T, Anderson J, Danielson L, Pohlson K, Remund T, Blears E, et al. Examination of near-wall hemodynamic parameters in the renal bridging stent of various stent graft configurations for repairing visceral branched aortic aneurysms. Journal of vascular surgery. 2015

6 Kandail H, Hamady M, Xu XY. Patient-specific analysis of displacement forces acting on fenestrated stent grafts for endovascular aneurysm repair. Journal of Biomechanics. 2014;47(14):3546-54

7 Avrahami I, Brand M, Meirson T, Ovadia-Blechman Z, Halak M. Hemodynamic and mechanical aspects of fenestrated endografts for treatment of Abdominal Aortic Aneurysm. European Journal of Mechanics B-Fluids. 2012;35:85-91.

8 Jones SM, Poole RJ, How TV, Williams RL, McWilliams RG, Brennan JA, et al. Computational fluid dynamic analysis of the effect of morphologic features on distraction forces in fenestrated stent grafts. Journal of vascular surgery. 2014;60(6):1648-56. e1

9 Ou J, Tang A, Chiu T, Chow K, Chan Y, Cheng S. Haemodynamic variations of flow to renal arteries in custom-made and pivot branch fenestrated endografting. European Journal of Vascular and Endovascular Surgery. 2017;53(1):133-9

10 Olufsen MS, Peskin CS, Kim WY, Pedersen EM, Nadim A, Larsen J. Numerical simulation and experimental validation of blood flow in arteries with structured-tree outflow conditions. Annals of biomedical engineering. 2000;28(11):1281-99

11 Reymond P, Merenda F, Perren F, Rufenacht D, Stergiopulos N. Validation of a one-dimensional model of the systemic arterial tree. American Journal of Physiology-Heart and Circulatory Physiology. 2009;297(1):H208-H22

12 Formaggia L, Gerbeau J-F, Nobile F, Quarteroni A. On the coupling of 3D and 1D Navier–Stokes equations for flow problems in compliant vessels. Computer methods in applied mechanics and engineering. 2001;191(6-7):561-82

13 Kim HJ, Vignon-Clementel IE, Figueroa CA, LaDisa JF, Jansen KE, Feinstein JA, et al. On Coupling a Lumped Parameter Heart Model and a Three-Dimensional Finite Element Aorta Model. Annals of Biomedical Engineering. 2009;37(11):2153-69

14 Stergiopulos N, Young D, Rogge T. Computer simulation of

arterial flow with applications to arterial and aortic stenoses. J Biomech. 1992;25(12):1477-88

15 Gallo D, Vardoulis O, Monney P, Piccini D, Antiochos P, Schwitter J, et al. Cardiovascular morphometry with high-resolution 3D magnetic resonance: First application to left ventricle diastolic dysfunction. Medical engineering & physics. 2017;47:64-71

16 Morbiducci U, Kok AM, Kwak BR, Stone PH, Steinman DA, Wentzel JJ. Atherosclerosis at arterial bifurcations: evidence for the role of haemodynamics and geometry. Thromb Haemost. 2016;115(3):484-92

17 Morbiducci U, Ponzini R, Rizzo G, Cadioli M, Esposito A, De Cobelli F, et al. In vivo quantification of helical blood flow in human aorta by time-resolved three-dimensional cine phase contrast magnetic resonance imaging. Annals of Biomedical Engineering. 2009;37(3):516-31

18 Morbiducci U, Ponzini R, Gallo D, Bignardi C, Rizzo G. Inflow boundary conditions for image-based computational hemodynamics: Impact of idealized versus measured velocity profiles in the human aorta. Journal of Biomechanics. 2013;46(1):102-9

19 Di Achille P, Tellides G, Humphrey J. Hemodynamics-driven deposition of intraluminal thrombus in abdominal aortic aneurysms. International journal for numerical methods in biomedical engineering. 2017;33(5):e2828

20 Papadopoulos KP, Gavaises M, Pantos I, Katritsis DG, Mitroglou N. Derivation of flow related risk indices for stenosed left anterior descending coronary arteries with the use of computer simulations. Med Eng Phys. 2016;38(9):929-39

21 Hardman D, Semple SI, Richards JM, Hoskins PR. Comparison of patient-specific inlet boundary conditions in the numerical modelling of blood flow in abdominal aortic aneurysm disease. International journal for numerical methods in biomedical engineering. 2013;29(2):165-78

22 Ou J, Chan Y-C, Chan CY-T, Cheng SW. Geometric alteration of renal arteries after fenestrated grafting and the impact on renal function. Annals of vascular surgery. 2017;41:89-95

23 Xiao N, Humphrey JD, Figueroa CA. Multi-scale computational model of three-dimensional hemodynamics within a deformable full-body arterial network. Journal of computational physics. 2013;244:22-40

24 Vignon-Clementel IE, Figueroa CA, Jansen KE, Taylor CA. Outflow boundary conditions for three-dimensional finite element modeling of blood flow and pressure in arteries. Comput Method Appl M. 2006;195(29-32):3776-96

25 Vignon IE, Taylor CA. Outflow boundary conditions for one-dimensional finite element modeling of blood flow and pressure waves in arteries. Wave Motion. 2004;39(4):361-74

26 Steele BN, Taylor CA, editors. Simulation of blood flow in the abdominal aorta at rest and during exercise using a 1-d finite element method with impedance boundary conditions derived from a fractal tree. Proceedings of the 2003 ASME Summer Bioengineering Conference; 2003

27 Blanco PJ, Feijóo RA. A 3D-1D-0D Computational model for the entire cardiovascular system. Computational Mechanics, eds E Dvorking, M Goldschmit, M Storti. 2010;29:5887-911

28 Crosetto P, Reymond P, Deparis S, Kontaxakis D, Stergiopulos N, Quarteroni A. Fluid–structure interaction simulation of aortic blood flow. Computers & Fluids. 2011;43(1):46-57

29 Papaioannou TG, Stefanadis C. Vascular wall shear stress: basic principles and methods. Hellenic J Cardiol. 2005;46(1):9-15

30 Boyd AJ, Kuhn DC, Lozowy RJ, Kulbisky GP. Low wall shear stress predominates at sites of abdominal aortic aneurysm rupture. Journal of vascular surgery. 2015;63(6):1613-9

31 Bluestein D, Dumont K, De Beule M, Ricotta J, Impellizzeri P, Verhegghe B, et al. Intraluminal thrombus and risk of rupture in patient specific abdominal aortic aneurysm - FSI modelling. Computer methods in biomechanics and biomedical engineering. 2008;12(1):73-81

32 Biasetti J, Hussain F, Gasser TC. Blood flow and coherent vortices in the normal and aneurysmatic aortas: a fluid dynamical approach to intraluminal thrombus formation. Journal of the Royal Society Interface. 2011;8(63):1449-61

33 Biasetti J, Gasser TC, Auer M, Hedin U, Labruto F. Hemodynamics of the normal aorta compared to fusiform and saccular abdominal aortic aneurysms with emphasis on a potential thrombus formation mechanism. Annals of Biomedical Engineering. 2010;38(2):380-90

34 Raptis A, Xenos M, Georgakarakos E, Kouvelos G, Giannoukas A, Labropoulos N, et al. Comparison of physiological and post-endovascular aneurysm repair infrarenal blood flow. Computer methods in biomechanics and biomedical engineering. 2017;20(3):242-9

35 Raptis A, Xenos M, Georgakarakos E, Kouvelos G, Giannoukas A, Matsagkas M. Hemodynamic profile of two aortic endografts accounting for their postimplantation position. Journal of Medical Devices. 2017;11(2):021003

36 Tasso P, Raptis A, Matsagkas M, Rizzini ML, Gallo D, Xenos M, et al. Abdominal Aortic Aneurysm Endovascular Repair: Profiling Postimplantation Morphometry and Hemodynamics With Image-Based Computational Fluid Dynamics. Journal of biomechanical engineering. 2018;140(11):111003

37 Liu X, Sun A, Fan Y, Deng X. Physiological significance of helical flow in the arterial system and its potential clinical applications. Annals of Biomedical Engineering. 2015;43(1):3-15